Sustainable Engineering Materials
ISSN: 3105-1960 (Print); ISSN: 3105-1979 (Online)
http://www.sustain-dpl.com/picnews.asp?id=177
DOI: 10.54113/j.suem.2025.000007

ORIGINAL ARTICLE

Sustainability assessment of marine RC structures containing mid to high volume supplementary cementitious materials

Sakib Hasnat, Tanvir Manzur*

Department of Civil Engineering, Bangladesh University of Engineering and Technology, Dhaka, Bangladesh
*Corresponding Author: Tanvir Manzur. Email: tanvirmanzur@ce.buet.ac.bd

Abstract: Reinforced Concrete (RC) structures in marine environments deteriorate rapidly due to chloride-induced corrosion, requiring performance-based mix and cover design for environmental sustainability and reduced life-cycle costs (LCC). A probabilistic performance-based framework is presented in this study to predict and compare the service life, LCC and equivalent carbon dioxide emissions (CO_2-e) of concrete mixes with different binder compositions in harsh marine exposures. Concrete mixes with varying proportions of supplementary cementitious materials (SCMs) like fly ash and slag were tested for strength, chloride diffusion, and electrical resistivity. Using the results, a probabilistic analysis was conducted on a typical coastal structure with a 50-year design service life considering a range of commonly practiced covers. The time-dependent failure probabilities for initiation and propagation were evaluated using Monte Carlo Simulation, applying patch repair when the first corrosion-induced crack appears. Material Sustainability Indicators (MSI) were assessed in terms of LCC and lifetime carbon emissions. The findings demonstrate that a 25% fly ash replacement notably enhanced the cost-effectiveness of structures by delaying the time to cracking and reducing the repair frequency. Combined with larger cover, high volume replacement led to a reduction of around 60% in CO_2 emissions. This research highlights the need for performance-based mix designs to minimize long-term costs and environmental impact for RC structures in harsh, marine exposure.

Keywords: reinforced concrete, chloride induced corrosion, life-cycle costs, cover thickness, service life, CO_2-e, supplementary cementitious materials

1 Introduction

Chloride induced corrosion is one of the frequent and major causes of reduction in service lives for Reinforced Concrete (RC) structures, which can lead to premature failure and economic liability due to excessive unforeseen repair and maintenance [1, 2]. The staggering annual cost of corrosion damage around the world is approximately US$2.5 trillion [3], underscoring the necessity for construction practices that will ensure durable and long-lasting structures. Most RC structures worldwide are approaching or exceeding 50 years of service, with those in marine environments exhibiting faster deterioration, often reaching serviceability and durability limit states such as cover cracking, spalling. Moreover, human-induced climate change will cause the eventual reduction in service lives of coastal RC structures [4]. This challenge is more severe in countries like Bangladesh, where the absence of durability oriented building codes and high climate vulnerability make RC structures in marine environments particularly prone to chloride ion ingress [5], ultimately causing

Received: 11 May 2025; Received in revised form: 23 August 2025; Accepted: 12 October 2025

reinforcement corrosion and subsequent damage.

Service lives of RC structures subjected to chloride induced corrosion comprise two phases: the initiation phase (T_i) and the propagation phase (T_{cr}) [6]. The initiation phase, T_i, denotes the time needed for chloride ions to reach the critical concentration [7], leading to de-passivation of the protective alkaline layer around the reinforcement, therefore, initiating corrosion. After initiation, the propagation phase, T_{cr}, marks the time period during which corrosion continues and cumulation of corrosion induced damage occurs until a limit state of cracking is reached, signifying the termination of the structure's service life, or the need for repair work to ensure continued functionality [8]. For maintenance operations, typical patchwork is common, where the cracked cover is replaced with pristine concrete. However, this approach is viable only up to a certain degree of degradation of the corroded reinforcement. Beyond this threshold, replacement of the damaged reinforcement becomes imperative for sustained operation. While this strategy is systematic, the cumulative costs and equivalent carbon emissions (CO_2-e) can become substantial depending on the frequency of required repairs throughout the structure's lifespan. It can be assumed that once corrosion initiates, it can continue indefinitely, resulting in the reinforcement area being reduced significantly.

Concrete is the most widely produced solid material globally, with its primary component, Ordinary Portland Cement (OPC), accounting for about 5-7% of annual global CO_2 emissions [9]. The global warming potential of concrete can be reduced significantly with the replacement of OPC with Supplementary Cementitious Materials (SCMs) such as fly ash and slag [10]. However, such strategies involving binder replacement may not be enough for the reduction of global CO_2 emissions caused by concrete production. Improper selection of binder materials can necessitate frequent repair operations, escalating long-term costs and carbon emissions. Effective corrosion management strategies are essential to extend the service life of RC structures and ensure reduced repair frequency. However, in order to assess the effectiveness and efficiency of these strategies, their life-cycle costs (LCC) and lifetime CO_2 emissions must be evaluated in the long run.

Typical strategies for extending service lives of RC structures and minimizing repair operations fall into two categories: preventing corrosion by use of corrosion-resistant reinforcement (epoxy-coated steel, stainless steel, fiber reinforced polymer composites (FRPC), etc.) [11] and delaying the onset of corrosion by employing alternative binder replacements (fly ash, slag, silica fume, etc.) [11, 12]. The effectiveness of these strategies in reducing the LCC for RC structures has been evaluated in existing literature in both deterministic and probabilistic terms. Some studies [9,13-15] adopted deterministic-based approaches in their repair frequency computations for different corrosion management strategies, without explicitly considering the uncertainties associated with service life analysis. In contrast, time-variant stochastic approaches incorporate these uncertainties more comprehensively, offering a broader perspective for designers and owners to select corrosion protection schemes based on chosen risk thresholds [16, 17]. Full probabilistic assessment of different reinforcement and binder alternatives has shown the effect of optimal binder selection in reducing the repair frequencies and consequently, the LCC and CO_2-e of RC structures in harsh environments [11, 12]. Crack repair by fly ash concrete has also been shown to lengthen the remaining service life and reduce the repair frequencies in RC structures [18]. Increasing concrete cover is also a crucial measure for improving the service life of RC structures in saline environments. Concrete cover acts as a cost-effective tool and is the most important parameter in reducing the number of repairs and extending the service lives of coastal structures [19], resulting in reduced life-cycle costs and environmental impacts [20]. Val and Stewart [21] have concluded that concrete cover can be a pivotal tool in reducing life-cycle costs for RC structures in coastal regions. However, there is a paucity in available published studies that have quantitatively examined the effects of supplementary cementitious materials (SCMs) combined with various clear covers in lengthening the lifespan of RC infrastructure and thereafter reducing their LCC and emissions in terms of equivalent carbon dioxide emissions (CO_2-e).

In this study, a comprehensive assessment of the suitability of some common concrete binders has been carried out in terms of service life, LCC, and CO_2-e of resulting RC structures in saline exposure. Lack of any performance-based guidelines in local codes [22-24] of the country for RC structures in harsh, marine environments has been a prerequisite for carrying out this research. The primary goal of this study is to compare the cost-effectiveness and environmental impact of local mixes combined with

various concrete covers in the construction and repair of a typical coastal structure within a lifespan of 50 years. To assess the economic and sustainability performance of different alternative binder types combined with a wide range of clear covers, a time-dependent probabilistic analysis has been performed considering both the initiation and the propagation phase and corresponding limit states. Patching has been assumed to be warranted when the failure probability surpasses a threshold, signifying the serviceability limit state, and is continued until the ultimate limit state (ULS) of failure is reached. The structure is assumed to have reached its ULS after the reinforcement area reduction exceeds a certain threshold percentage. After calculating the LCC and the CO_2-e for the structure within the 50-year service period, the Material Sustainability Indicators (MSIs) have been determined. The MSIs have been used to identify optimum mix design and cover combinations that can produce cost-effective and sustainable RC structures in chloride-prone regions.

2 Materials and Concrete Mix Design

The concrete mixes in this study were prepared with Ordinary Portland Cement (OPC), and different replacement levels of fly ash and/or slag as supplemental binders. The specific gravity and unit weight of OPC were 3.15 and 1440 kg/m^3, respectively. Class F fly ash [25] and blast furnace slag served as SCMs for this research. The chemical compositions of the binders, as determined by X-ray fluorescence (XRF) analysis, are shown in **Table 1**. For this study, 19 mm crushed stone chips and local sand known as 'Sylhet Sand' were utilized as coarse and fine aggregates. The fundamental properties of the aggregates, as determined through standard tests, are provided in **Table 2**. The aggregate sieve analysis results are illustrated in **Fig. 1**.

Table 1. Chemical composition of cementitious materials used.

Oxides	Mass%		
	OPC	Fly Ash	Slag
CaO	67.33	2.66	49.1
SiO_2	17.06	63.54	31.4
SO_3	4.57	0.28	2.09
Fe_2O_3	3.55	6.41	0.54
Al_2O_3	2.90	18.68	8.46
MgO	2.54	1.10	6.35
K_2O	1.30	2.89	0.53
TiO_2	0.42	2.39	0.94
SrO	0.092	0.055	0.07
Na_2O	0.077	0.32	0.19

Table 2. Properties of coarse and fine aggregates.

Tests	Specification	Coarse Aggregate	Fine Aggregate
Absorption Capacity		1.6%	0.9%
Unit Weight	ASTM C29 [29]	1488 kg/m^3	1572 kg/m^3
Apparent Specific Gravity		2.69	2.64
Bulk Specific Gravity (Oven-Dry Basis)	ASTM C127 [27] ASTM C128 [28]	2.63	2.56
Bulk Specific Gravity (SSD Basis)		2.67	2.59
Aggregate Crushing Value	BS 812-110:1990 [30]	22	-
Fineness Modulus	ASTM C136[32]	7.15	2.82
Los Angeles Abrasion Value	ASTM C131 [31]	30%	-

For this research, the concrete mix design was done following the guidelines from the ACI Mix Design Manual [26]. Concrete mixes were prepared with various replacement portions of SCMs (fly ash and slag) to evaluate their effect on the durability enhancement of concrete. To represent local construction practices, the slump was chosen to vary between 75 and 100 mm, and the varying water-to-binder ratios (*w/b*) were chosen to be 0.40, 0.46, and 0.57, representing commonly practiced specified design strengths of 35 MPa, 28 MPa, and 21 MPa, respectively. The mixes included two with fly ash replacing 25% and 35% of OPC, one with 40% slag replacement, two ternary mixes with a total

replacement of 40% (20% fly ash and 20% slag), and 50% (30% fly ash and slag), and a control mix with only OPC. This resulted in a total of 18 concrete mixes. Fly ash is denoted by FA, and slag is denoted by S, for the purpose of identifying the mixes. The concrete mixes were cast into standard 100 mm x 200 mm cylindrical molds. A summary of the mix plan with the different mix parameters is presented in **Table 3**. The mix design data, along with the mix designations and detailed quantities of all the constituents, are provided in **Table 4**.

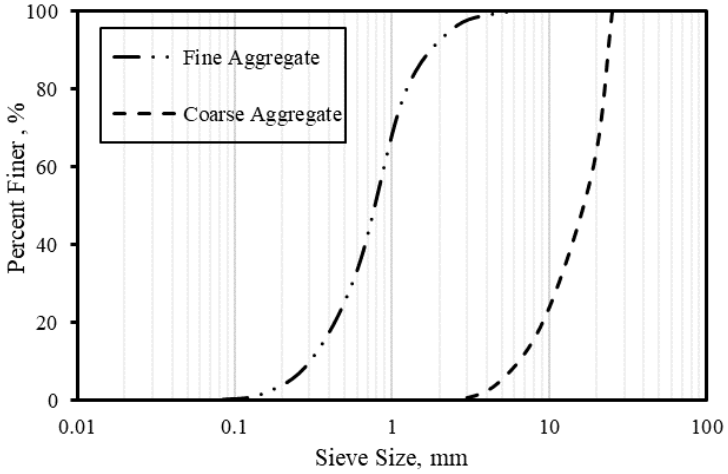

Fig. 1. Sieve analysis results of aggregates used in this study.

Table 3. Summary of all the mix design variables.

Water-Binder (*w/b*) Ratio	Target Slump (mm)	Type of Binder	Concrete Cover (mm)
0.40, 0.46, 0.57	75-100	100% OPC 75% OPC+25% FA 65% OPC+35% FA 60% OPC+40% S 60% OPC+20% FA+20% S 50% OPC+30% FA+20% S	37.5, 50, 62.5, 75

3 Experimental Program

To assess the mechanical and durability properties of the mixes, the concrete samples underwent a wide variety of tests. Slump tests [33] were performed on fresh concrete paste to confirm that the mixes were within the target 75-100 mm slump range. Additionally, compressive strength was determined, along with durability tests such as the electrical resistivity test and the Rapid Chloride Migration (RCM) test. These tests aided in assessing the mechanical performance of various concrete mixes, as well as evaluating their ability to extend the service life of RC infrastructure in harsh, chloride-laden environments.

3.1 Compressive Strength Test

To measure the compressive strength of the various concrete mixes as a key performance indicator, the specimens' strengths were assessed following the guidelines of ASTM C39 [34]. The cylindrical concrete samples were cured for 28 days, and their compressive strengths were tested at both 28 days and 180 days. For each measurement, the average strength of three concrete cylinders was recorded.

3.2 Rapid Chloride Migration (RCM) Test

The resistance of the concrete matrix to the movement of chloride ions is usually represented by the chloride diffusion coefficient (D_{rcm}). D_{rcm} of all concrete mixes was determined by subjecting the concrete specimens to a non-steady state RCM test following the guidelines of Nordtest Method NT BUILD 492 [35]. A schematic illustration of the arrangement is presented in **Fig. 2a**. For this test, the concrete cylinders were kept submerged for a duration of 180 days. At the time of the tests, the cylinders

were taken out of curing, and three sawn concrete disk samples, sized 100 mm by 50 mm, were produced from separate standard concrete cylinders. The disk specimens were extracted from the middle section of the cylindrical specimens. The sides of the disks were coated with black water-repellent paint. The concrete disks underwent a vacuum saturation procedure outlined in the standard, in a saturated $Ca(OH)_2$ solution, after which, the samples were kept in the same solution, completing the 24 hr preconditioning process. The disk specimens were then subjected to an electrical potential for a certain duration as per the standard [35]. After which, the disks were split, and an $AgNO_3$ solution was sprayed on the interior cross-section of the specimen. The depth of chloride penetration was identified by the visible white silver chloride precipitate (**Fig. 2b**). The chloride diffusion coefficient (D_{rcm}) was then determined using the anolyte temperature, specimen thickness, the applied voltage, test duration, and the average chloride penetration depth. The D_{rcm} determined from this test method is used as a parameter in the probabilistic service life modelling of the initiation period, along with other variables.

Table 4. Concrete mix details (per m^3 of mix).

Mix Designation	Proportion of SCMs	Coarse Aggregate (kg)	Total Binder (kg)	Fine Aggregate (kg)
Water/Binder Ratio: 0.40				
OPC	OPC (100)	1002	513	630
F25	OPC-FA (75-25)	1002	513	602
F35	OPC-FA (65-35)	1002	513	592
S40	OPC-S (60-40)	1002	513	615
F20S20	OPC-FA-S (60-20-20)	1002	513	600
F30S20	OPC-FA-S (50-30-20)	1002	513	588
Water/Binder Ratio: 0.46				
OPC	OPC (100)	1002	449	686
F25	OPC-FA (75-25)	1002	449	666
F35	OPC-FA (65-35)	1002	449	656
S40	OPC-S (60-40)	1002	449	677
F20S20	OPC-FA-S (60-20-20)	1002	449	655
F30S20	OPC-FA-S (50-30-20)	1002	449	646
Water/Binder Ratio: 0.57				
OPC	OPC (100)	1002	360	754
F25	OPC-FA (75-25)	1002	360	739
F35	OPC-FA (65-35)	1002	360	731
S40	OPC-S (60-40)	1002	360	748
F20S20	OPC-FA-S (60-20-20)	1002	360	737
F30S20	OPC-FA-S (50-30-20)	1002	360	729

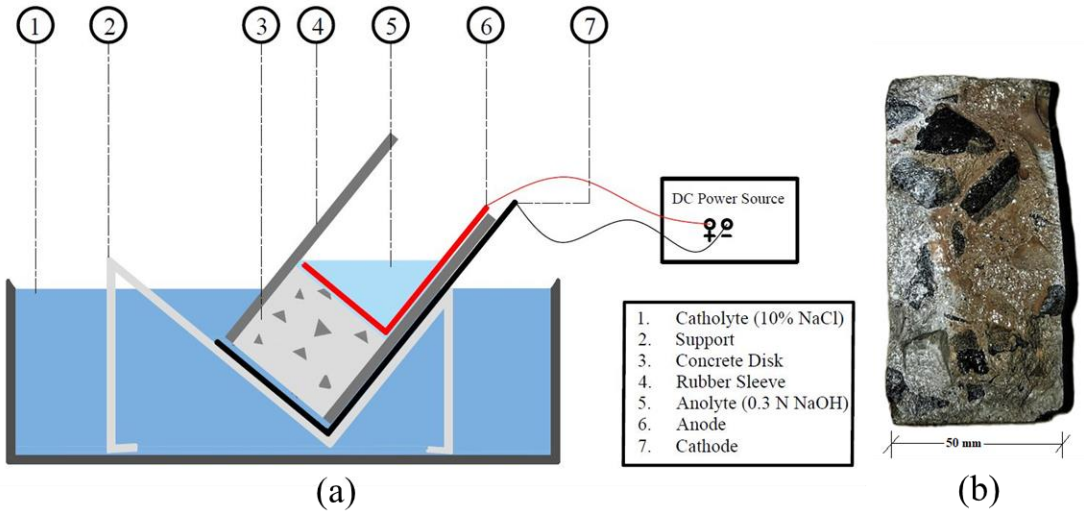

Fig. 2. (a) Schematic illustration of the migration test setup and (b) Formation of white silver chloride precipitate to indicate the depth of chloride penetration.

3.3 Electrical Resistivity Test

The electrical resistivity of all the concrete mixes was measured as an indicator of their durability performance [36], and also as an input parameter for the prediction of corrosion rates used in the modelling of the propagation period.

The surface electrical resistivity test, also known as the Wenner Four-Probe test [37] involves sending an electrical current through two outer probes and then measuring the resulting voltage difference between two inner electrodes (**Fig. 3a**). The test was performed in accordance with AASHTO T 358-15 [38] using the Proseq Resipod (**Fig. 3b**). The test specimens were fully submerged in water from the time they were demolded until the date of testing at 180 days. After the initial experimental readings, several correction factors were applied to account for the geometry of the specimen [37], effect of temperature [39], and saturation level [40]. The specific details regarding the application of these factors are described elsewhere [41], and are not included in this article.

Fig. 3. (a) Schematic illustration of surface resistivity measurement using the Wenner Four-Probe method and (c) Surface resistivity measurements using the Proseq Resipod.

4 Service Life Analysis

4.1 Time to Corrosion Initiation

As discussed earlier, the service life of an RC structure, exposed to chloride ion ingress, can be conceptually divided into two phases [6], the initiation phase (T_i) and the propagation phase (T_{cr}).

The time to corrosion initiation can be defined as the time needed for chloride ions to reach the steel-cementitious interface and de-passivate the alkaline protective layer surrounding reinforcement, thereby initiating corrosion. Following the Fick's 2nd law of diffusion, the chloride concentration ($C_{x,t}$) at a depth can be expressed by Eq. (1) and Eq. (2), as described in the fib Bulletin no. 34 [42].

$$C(x,t) = C_o + \left(C_{s,\Delta x} - C_o\right) \cdot \left[1 - erf \frac{x_c - \Delta x}{2 \cdot \sqrt{K_e \cdot K_t \cdot D_{rcm(t_o)} \cdot \left(\frac{t_o}{t_1}\right)^m t_i}}\right] \quad (1)$$

$$K_e = \exp\left[b_e \left(\frac{1}{T_{ref}} - \frac{1}{T_{real}}\right)\right] \quad (2)$$

In order to evaluate the suitability of the mixes in harsh marine exposures, the tidal, splash, and spray exposure conditions were considered in this analysis, which is also denoted as the XS3 exposure class in the fib guidelines [43]. The de-passivation of the alkaline protective layer is assumed to occur as soon as the threshold chloride concentration (C_{th}) is reached at the level of the reinforcement. The corresponding limit state for this criterion can be expressed as Eq. (3).

$$g_1(x,t) = C_{th} - C(x,t) \quad (3)$$

Where the limit state function is denoted as 'g_1(x,t)', the threshold chloride concentration is 'C_{th}', and the chloride concentration at time 't' at depth 'x' (reinforcement depth), is represented by 'C(x,t)'. The time to corrosion initiation is denoted by 'T_i' in Eq. 2. The values of the aging exponent, represented by 'm', for OPC, fly ash and slag have been used as recommended in the fib guidelines [43]. However, there are limited resources available for the aging exponent values for ternary mixes. Rengaraju *et al.* [44] reported that higher values in the order of 0.55~0.70 have been obtained for high volume SCM replacements. For this study, the aging exponent of the ternary mixes is considered to be the same as for fly ash, with a mean value of 0.60 and a standard deviation of 0.15, respectively, following a Beta distribution. The stochastic and deterministic parameters used in Eq. (2) to Eq. (4) are detailed in **Table 5**.

Table 5. Descriptions of the different parameters in Eq. (1), (2) and (3).

Parameters	Description	Distribution	Mean	Standard Deviation
C_{th}	Threshold chloride content (wt-%/binder) [42]	Beta	0.60 (*l.b.*: 0.20, *u.b.*: 2.0)*	0.15
C_o	Initial chloride content (wt-%/binder) [42]	Constant	0	-
$C_{s,\Delta x}$	Surface chloride content (wt-%/binder) [42]	Lognormal	3	1.35
x_c	Depth of concrete cover (mm) [43]	Lognormal	37.5, 50, 62.5, 75	8
Δx	Convection zone (mm) [42]	Beta	10 (l.b.: 0, u.b: 50)	5
K_t	Transfer parameter [42]	Constant	1	-
t_o	Reference age (years)	Constant	0.4932 (180 days)	-
D_{rcm}	Non-steady state migration coefficient of chloride through the concrete cover (m^2/s) [35]	Normal	As determined from RCM tests following NT BUILD 492 [35]	
m	The aging exponent [42]	Beta	OPC: 0.30 Fly ash: 0.60 Slag: 0.45 Fly ash+Slag:0.60 (l.b.: 0.0, u.b.: 1.0)	OPC: 0.12 Fly ash: 0.15 Slag: 0.20 Fly ash+Slag: 0.15
b_e	A regression variable (K) [42]	Normal	4800	700
T_{ref}	A reference temperature (K) [42]	Constant	293	-
T_{real}	Ambient temperature (K), taken for Cox's Bazar, a coastal city of Bangladesh [45]	Normal	299	5

**u.b.*: Upper bound and *l.b.*: Lower bound of the Beta distribution.

4.2 Time to Cracking of Concrete Cover

The first sign of a corrosion crack in an RC structure typically marks the end of its functional service life, at which point the affected structural components require repair and rehabilitation [8]. The time to corrosion cracking has been predicted by many authors [46-49]. In this study, the analytical model used for modeling the crack initiation is based on the thick-walled cylinder approach by Maaddawy and Soudki [46], schematically represented in **Fig. 4**. Although the analytical model assumes a perfectly plastic failure of concrete, it is able to produce satisfactory and conservative predictions compared to other analytical and numerical models [50, 51]. As shown in **Fig. 4** adapted from Ref. [46], 'D' is considered as the diameter of the reinforcement bar, and 'δ_o' as the porous zone thickness. The required radial pressure, P_c in order to produce a concrete displacement δ_c for accommodating corrosion products can be expressed by Eq. (4) [52].

$$P_c = \frac{2\frac{M_{loss}}{\rho_s}E_{ef}(\alpha_v - 1)}{\pi D(1+\Psi+\nu)(D+2\delta_o)} - \frac{2\delta_o E_{ef}}{(1+\Psi+\nu)(D+2\delta_o)} \quad (4)$$

Where 'Ψ' can be defined as Eq. (5), where 'D^*' can be defined such that, $D^*=D+2\delta_o$ and 'x_c' is the wall thickness of the cylinder, which is identical to the concrete cover.

$$\Psi = \frac{D^{*2}}{2x_c(x_c + D^*)} \tag{5}$$

And the tensile stress, P_{ct} required to cause cracking of the concrete cover can be expressed by Eq. (6) [46].

$$P_{ct} = \frac{2x_c f_{ct}}{D} \tag{6}$$

Where 'f_{ct}' represents the tensile strength of concrete. The mass loss M_{loss} (gm/m) of the reinforcement is expressed as Eq. (7).

$$M_{loss} = 2.315\times10^{-4} \cdot \pi \cdot D \cdot i_{corr} \cdot T_{cr} \cdot 31536000 \tag{7}$$

Where 'T_{cr}' is the time passed between the initiation of corrosion and the cracking of concrete cover (years). In Eq. (7), the corrosion rate 'i_{corr}' was estimated using the model proposed by Pour-Ghaz *et al.* [53], which defines independent relationships between steel corrosion rate, ambient temperature, concrete resistivity, kinetic factors, and limiting current density. The electrical resistivity of concrete represents the tortuosity of the concrete matrix and is a predominant property controlling the corrosion rate of the reinforcing steel [6, 54]. The model [53] incorporates the experimental resistivity values as input and has shown good agreement with other experimental and field results as well [55, 56]. The Pour-Ghaz model offers a more representative approach for simulating corrosion in high-humidity conditions typical of coastal regions. While local experimental validation data were not available, the model's applicability was supported by a validation study [56], which demonstrated good agreement with data from a wide range of relative humidity, even up to full saturation, and high-humidity temperate regions, which reinforces the applicability to the current study's environmental context.

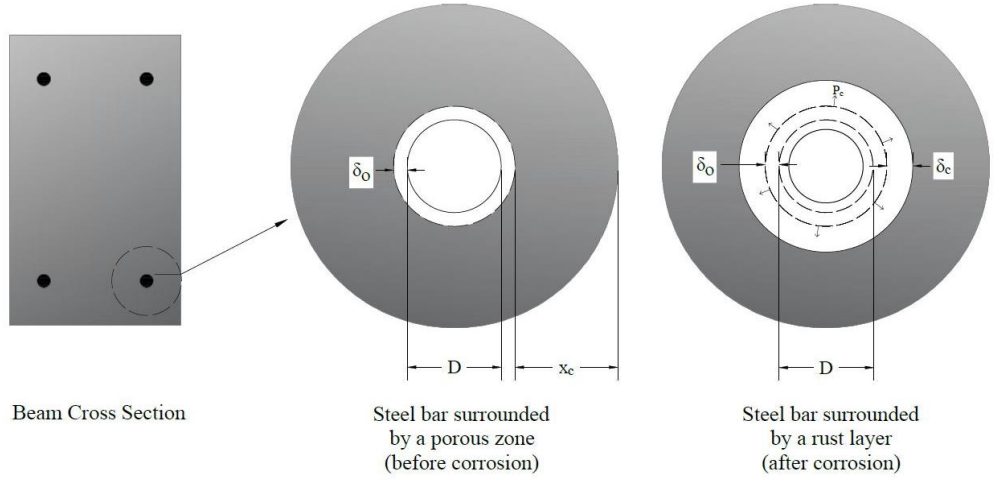

Fig. 4. Details of the thick-walled cylinder model, adapted from Ref. [46].

The concrete cover crack with the radial expansion stress P_c exceeding the tensile strength of concrete, P_{ct}. Considering the serviceability limit state as the time at which the concrete cover cracks due to corrosion-induced damage, the limit state for this criteria can be expressed as Eq. (8).

$$g_2(x,t) = P_{ct} - P_c(x,t) \tag{8}$$

Where 'P_c(x, t)' represents the radial expansion stress due to corrosion products at time 't'. The deterministic and stochastic parameters used in Eq. (4), Eq. (6), and Eq. (7) are presented in **Table 6**, along with their relevant descriptions, distributions, means, and standard deviations.

4.3 Probabilistic Analysis

Recalling the limit state functions defined in Eq. (3) and Eq. (8), the probabilities of failure for the

initiation of corrosion '$P_{f(i)}$' and the initiation of cracking '$P_{f(cr)}$' can be defined by Eq. (9) and Eq. (10).

$$P_{f(i)} = P\left[g_1(x,t) < 0\right] \tag{9}$$

$$P_{f(cr)} = P\left[g_2(x,t) < 0\right] \tag{10}$$

The inherent variability of the parameters in service life analysis necessitates the adoption of a probabilistic approach. A schematic of the probabilistic service life analysis framework has been presented in **Fig. 5**. The Monte Carlo Simulation (MCS) method with 100,000 iterations was applied in the stochastic analysis to evaluate the limit state functions stated in Eq. (9) and Eq. (10). The parameters listed in **Tables 5** and **6** were used to compute the time-dependent failure probabilities of the different mixes. For the initiation period (T_i), the failure probability ($P_{f(i)}$) for the limit state of de-passivation (Eq. 3) is chosen to be 10% (reliability index, β=1.28), as per the fib Bulletin 34 [42]. Due to uncertainties in the propagation period [8], unlike the initiation period models, a lower failure probability is recommended for estimating the time to cracking (T_{cr}) in total service life. Therefore, the failure probability ($P_{f(cr)}$) for cracking is set at 6.7% (reliability index, β=1.5), as recommended by DuraCrete [57] for the limit state of cracking and spalling. Hence, the total time to cracking can be written as,

$$T_L = T_i + T_{cr} \tag{11}$$

Table 6. Descriptions of the different parameters used in Eq. (4), (6) and (7).

Parameters	Description	Distribution	Mean (μ)	Standard Deviation (σ)
E_c	Elastic modulus of concrete (MPa) [58]	Normal	$4733\sqrt{(f}c)$*	0.12μ
f_{ct}	Tensile strength of concrete (MPa) [58]	Normal	$0.6227\sqrt{(f}c)$	0.20μ
N	Poisson's ratio of concrete [46]	Constant	0.20	-
φ_c	Creep coefficient of concrete [46]	Constant	2.35	-
D	Rebar diameter (mm)	Constant	10	-
ρ_s	Mass density of steel (gm/m^3)	Constant	7850000	-
α_v	Relative volume ratio [16]	Beta	3.01 (l.b.: 1.695, u.b.: 6.3)*	0.8097
δ_o	Porous zone thickness (m) [16]	Uniform	l.b.: 5E-06, u.b.: 12E-05	0.53μ
x_c	Depth of concrete cover (mm) [42]	Lognormal	37.5, 50, 62.5, 75	8
i_{corr}	Corrosion rate of steel (μA/cm^2) [59]	Lognormal	As determined from [53]	0.34μ

*fc: 28-day compressive strength of concrete determined from standard tests, u.b.: Upper bound and l.b.: Lower bound of the Beta distribution.

5 Principles of Life-Cycle Cost Analysis

Life-cycle cost (LCC) analysis has been used as a tool to assess and compare the cost-effectiveness of the different binder types and cover thicknesses following ASTM E917 [60] standards. The LCC of an RC structure consists of initial construction costs (C_c), maintenance costs (C_m) in the structure's service life, and end-of-life turnover for the RC structure. The initial construction costs cover the cost of the materials (reinforcement and binder), labor, transportation, and general construction. However, for this study, labor, transportation, and general construction costs have been assumed constant across alternatives [9]. The maintenance costs, 'C_m' account for periodic inspections, minor rehabilitation, and repair. In this study, only repair costs incurred due to corrosion induced cracking have been considered; periodic inspections and minor rehabilitations have been assumed equal for all alternatives [14].

The repair cost, in this case, has been assumed to be the cost of simple patchwork, in which the serviceability of the RC structure is restored by replacing the contaminated concrete beyond the reinforcement level. This patchwork is warranted when the first crack appears and is continued in periodic intervals until the ultimate limit state (ULS), represented by the reinforcement area reduction exceeding 10% [11]. The service life of each repair interval has been assumed to align with the duration of the propagation period, and repair is applied again when the serviceability limit state is exceeded, and so on. The end-of-life turnover has also been assumed to be the same for all the design alternatives

in this study. Thus, the total LCC incurred over a service life period '*T*', calculated based on the initial materials cost and maintenance costs, in terms of present worth, can be expressed as Eq. (12) [60].

$$LCC = C_c + \sum_{t=1}^{T} \frac{C_m (1+i)^t}{(1+r)^t} \tag{12}$$

Here, '*i*' represents the inflation rate, representing the annual rate at which the price of goods and services will increase in the long run, and '*r*' is the annual rate at which future costs are discounted to base-year costs, net of the inflation rate. The inflation and discount rates used have been obtained from the annual rates averaged over the last 10 years for Bangladesh. These average rates are 6.2% and 4.52% for i and r, respectively, obtained from Ref. [61].

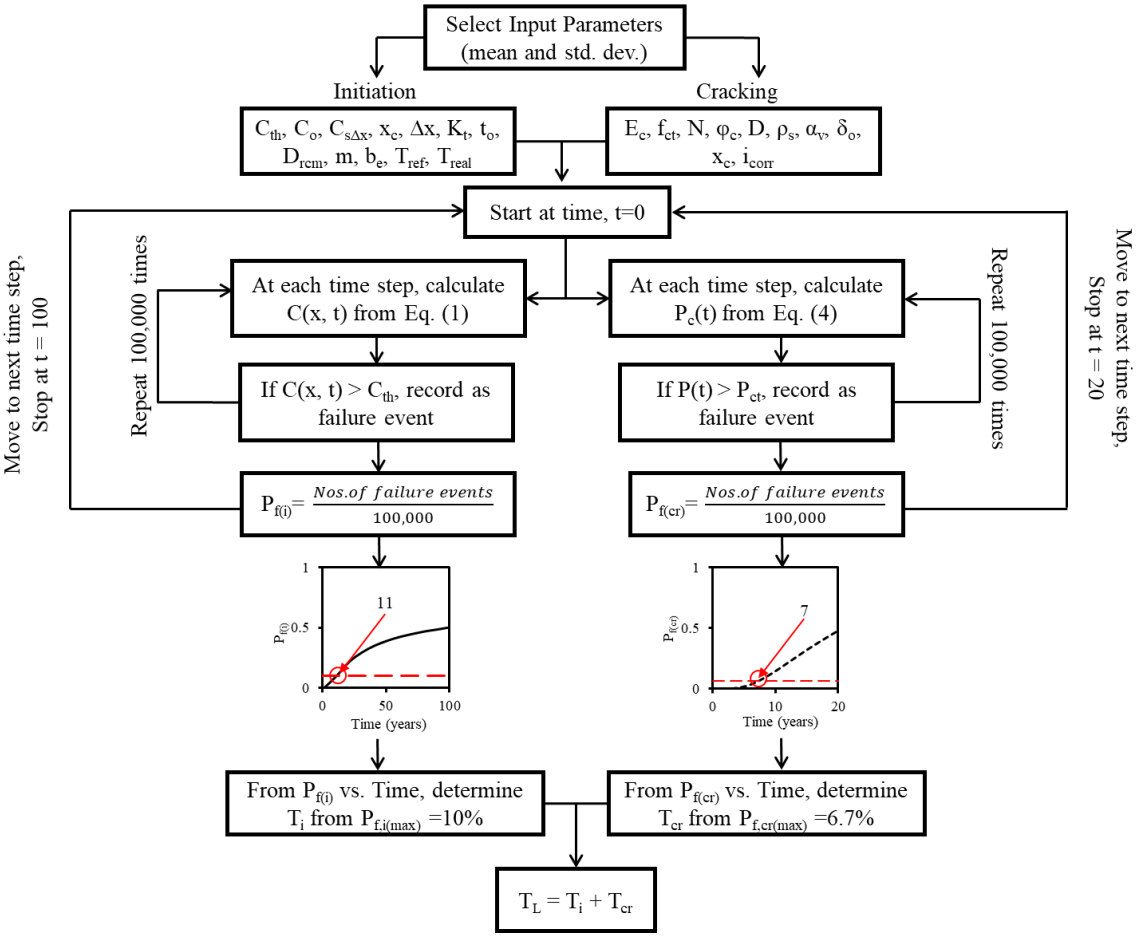

Fig. 5. Schematic illustration of the probabilistic analysis framework for service life analysis.

6 Estimation of Embodied CO_2

The total embodied equivalent carbon footprint of concrete from cradle to grave, '*E*' (CO_2-e) for the produced concrete mixes and cover combinations has been calculated based on Eq. (13).

$$E = \sum M \times EF \tag{13}$$

Where the total material amount (in tons) is denoted by '*M*' and the CO_2 emission factor used for cement, fly ash and slag is denoted by '*EF*'. OPC has an emission factor of 0.913 t CO_2-e/t [62] while fly ash and slag have much lower factors of 0.027 t CO_2-e/t [63] and 0.022 t CO_2-e/t [62], respectively. The embodied CO_2 for the mixes was calculated based on these emission factors. A 50-year service life counterfort retaining wall with varying covers (37.5 mm to 75 mm) is used as a case study. Further discussion on the illustrative example is provided in later sections. The lifetime CO_2 emissions of a coastal RC structure comprise the initial emissions from construction and the additional emissions generated through routine maintenance activities [64]. Emission factors for sand and crushed stone have been ignored since their values are negligible compared to those of OPC, fly ash, and slag [65]. The

emission factors for natural sand and crushed stone are approximately 0.0066 t CO_2-e/t and 0.0085 t CO_2-e/t [65], respectively, over 100 times lower than the emission factor for OPC. Thus, exclusion of these factors has minimal influence on comparative sustainability results. The CO_2-e for each patchwork operation is determined based on the materials necessary to replace the damaged concrete with concrete having a similar quality to that of the original structure.

7 Results and Discussions

7.1 Experimental Results

The experimental results of the chloride diffusion coefficient, electrical resistivity and compressive strength have been presented in **Table 7** for the different mixes in this study.

Regarding the degree of corrosion vulnerability of the mixes, the electrical resistivity and D_{rcm} present useful insights. From **Table 7**, it is clearly evident that the mixes containing OPC only exhibited notably inferior performance in terms of both resistivity and D_{rcm} than the mixes incorporating SCMs. SCMs, at any replacement level, reduce corrosion susceptibility, increasing resistivity and lowering D_{rcm} across all design strengths [66]. The mixes with 25% fly ash (F25) yielded the lowest diffusion coefficients and the highest resistivity. A slight increment of fly ash from 25% to 35% led to reduced durability. Although this finding diverges from the results reported by some studies [23, 41], similar results have been reported by other researchers [67]. Mixes with 40% slag performed better than OPC, but not as well as F25 and F35. Ternary mixes, particularly F30S20, exhibited higher resistivity and lower D_{rcm} than the 40% slag mix. The measurements presented for D_{rcm} and electrical resistivity were made at the age of 180 days, representing the long-term tortuosity of the cementing mixes.

Regarding compressive strength results, most of the mixes containing SCMs generally fell short of the 28-day design strength, while OPC-only mixes performed as anticipated. However, the SCM mixes showed substantial strength improvements at the extended age of 180 days, eventually achieving the specified design strength. It was evident that the slag-only mixes surpassed the strengths of all the other SCM mixes at earlier ages, likely due to the higher CaO content (49%) in slag relative to fly ash (2.7%), consistent with other studies as well [23]. However, the S40 mix underperforms the fly ash mixes in terms of long-term durability indicators such as the D_{rcm} and the electrical resistivity. This difference can be attributed to the distinct hydration mechanisms of slag and fly ash. Slag contributes to early strength through earlier accelerated hydration and C-S-H formation [68]. In contrast, the slower pozzolanic reaction of fly ash leads to the formation of secondary C-S-H at later ages, which is amorphous in nature. This results in continued pore refinement and improved resistance to chloride ingress at later ages [69, 70]. As a result, the F25 mixes exhibit better durability performance at 180 days compared to the slag mixes. For the ternary mixes, F20S20 performed better than F30S20, possibly due to the higher replacement ratio (50%) of the latter mix. Notably, the ternary mixtures tend to exhibit slightly lower strengths at later ages compared to pure fly ash or slag mixes. However, the early age strengths of the F20S20 mixes were higher than those of the F25 and F35 mixes.

7.2 Probabilistic Service Life Analysis

The service life analysis, based on probabilistic calculus, considers the XS3 exposure class (tidal, splash, and spray zones) and Cox's Bazar, a coastal area in Bangladesh with significant infrastructure growth. The necessary data for the mentioned location has been sourced from available information [45]. While the temperature, humidity, and exposure condition inputs are specific to the coastal regions of Bangladesh, the probabilistic modeling approach, including the service life framework and LCC, CO_2-e calculation, remains adaptable to other temperate marine climates. By modifying the environmental parameters in the probabilistic framework, the approach can be applied to diverse marine environments with different climatic conditions. Since the concrete cover plays a crucial role in the enhancement of service life performance of RC structures [42], a range of typical cover thicknesses was chosen in this study for the purpose of analysis (i.e., 37.5 mm, 50 mm, 62.5 mm, and 75 mm). Although local codes recommend a 75 mm cover for extreme conditions [71], poor construction practices often result in lower covers, increasing the risk of degradation. Additionally, a 75 mm cover may not sufficiently prolong service life for all binder types.

Table 7. Experimental results of the mixes considered in this study.

Mix Designation	Chloride Diffusion Coefficient (10^{-12} m^2/s)	Electrical Resistivity (kΩ.cm)	Compressive Strength (MPa)		Specified Design Strength (MPa)
			28d	180d	
W/B ratio: 0.40					
OPC	4.73±0.90	10.42±1.67	45.4	52.7	35
F25	1.62±0.37	27.48±5.22	29.3	51.9	
F35	1.79±0.38	24.96±4.24	26.0	48.6	
S40	2.40±0.57	20.72±2.92	33.4	50.5	
F20S20	2.34±0.45	17.48±2.79	31.4	46.0	
F30S20	2.57±0.59	23.41±3.92	23.9	43.7	
W/B ratio: 0.46					
OPC	5.37±1.18	9.73±1.95	43.3	50.6	28
F25	1.73±0.43	24.54±3.93	26.2	48.1	
F35	2.40±0.44	20.97±3.77	25.1	42.2	
S40	3.52±0.67	13.41±2.55	29.4	44.2	
F20S20	2.89±0.69	16.31±2.61	26.5	36.7	
F30S20	2.60±0.60	22.06±3.09	18.1	31.3	
W/B ratio: 0.57					
OPC	7.48±1.65	9.57±1.44	36.1	42.8	21
F25	2.63±0.55	21.71±4.34	20.6	35.6	
F35	3.00±0.56	16.34±3.10	16.7	31.0	
S40	4.90±1.12	11.68±1.99	23.8	37.7	
F20S20	3.24±0.81	14.25±2.28	20.6	32.1	
F30S20	2.85±0.54	18.30±2.75	13.2	23.8	

A sample of the computed curves from the probabilistic calculus for the 28 MPa design strength category (*w/b* ratio = 0.46) has been presented in **Fig. 6** and **Fig. 7**. For **Fig. 6a** and **Fig. 7a**, a single cover thickness of 62.5 mm is selected for all mixes considered, and **Fig. 6b** and **Fig. 7b** illustrate the impact of cover increment on the F35 for both the initiation and propagation stage. From **Fig. 6a**, it is evident that blended mixes perform substantially better than the OPC mix in terms of T_i. For a 62.5 mm cover, corrosion could begin around 3 years after construction in OPC mixes, but nearly 60 years for the F25 mix. Notably, the F25 mixes have demonstrated the most favorable performance across all cover thicknesses, which is anticipated given the lowest D_{rcm} value (1.73×10^{-12} m^2/s) of F25 within the considered design strength category. The superior performance of fly ash-containing mixes, including ternary mixes, is attributed to the long-term pore refinement action of the amorphous silica (63.5%) present in the cementitious matrix due to the addition of fly ash. The pozzolanic activity of fly ash results in the formation of secondary Calcium Silicate Hydrate (C-S-H) gel, which results in a denser microstructure, hindering the movement of chloride ions through the concrete matrix [70]. As for the slag-only mix, the C-S-H gel formation takes place as soon as the calcium silicate glass in slag was dissolved in the alkaline pore solution provided by the initial hydration reactions of OPC [68, 72, 73]. This is the reason for the aging exponent (m) of slag-only mixes to be considered as 0.45 and the mixes containing fly ash to be considered as 0.60. The higher the value of the 'm', the longer the hydration reaction will continue, resulting in a denser microstructure. Concrete cover significantly impacts the T_i for various mixes [17, 44], which is evident from **Fig. 6b**. For the F35 mix, increasing the cover thickness from 37.5 mm to 75 mm extended T_i from 1.5 years to 98 years. However, the lower pore refinement and aging exponent of OPC and S40 reduce the effectiveness of the cover increment. Even with a 75 mm cover, corrosion initiates within 4 years for OPC and 21 years for S40.

Fig. 7 presents a sample of the probabilistic calculus for the crack propagation period, i.e. the time taken for the concrete cover to crack after corrosion initiation. From **Fig. 7a**, it is evident that SCM replacements significantly improve T_{cr} compared to OPC. The idea that the crack propagation period does not depend on the selected binder types has been suggested by some researchers previously [74], which has led to the general assumption of a lump-sum estimate of T_{cr}. However, the probabilistic calculations presented show that the post-corrosion initiation service life of RC structures can be extended up to 11 years (F25 mix, 75 mm cover) by SCM replacement, whereas OPC struggles to reach

a 5-year T_{cr}, even at 75 mm cover. From **Fig. 7b**, it can be seen that the concrete cover is also a controlling parameter for T_{cr}. For the F35 mix, doubling the cover thickness from 37.5 mm to 75 mm increases T_{cr} from 4 to 10 years, a trend observed in all mixes. A thicker cover requires more tensile force to crack it, requiring a larger accumulation of corrosion products and hence, taking more time [75]. Additionally, the corrosion rate also varies inversely with the cover thickness [53], showing the effect of concrete cover in lengthening T_{cr}.

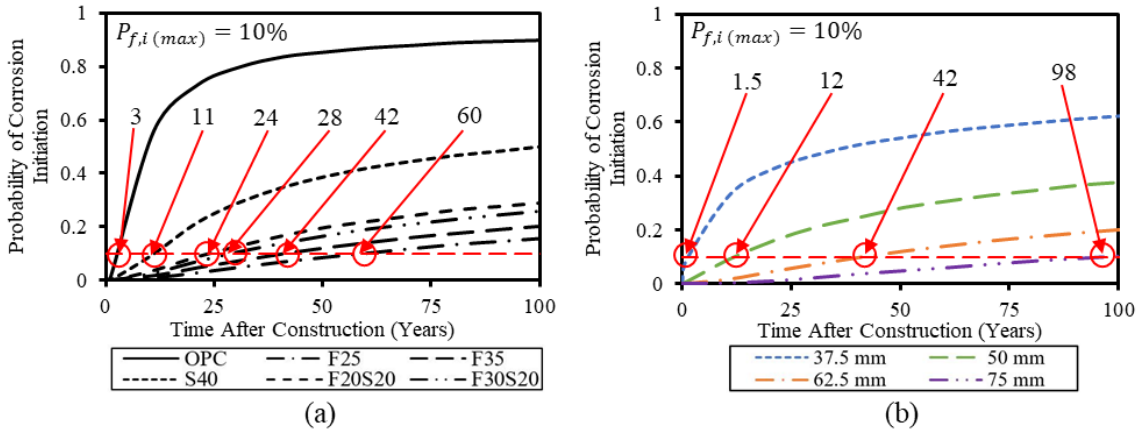

Fig. 6. Time-variant probabilities of failure ($P_{f(i)}$) for the initiation period for (a) All mixes considered and cover of 62.5 mm and (b) All covers considered and F35 mix for *w/b* ratio=0.46.

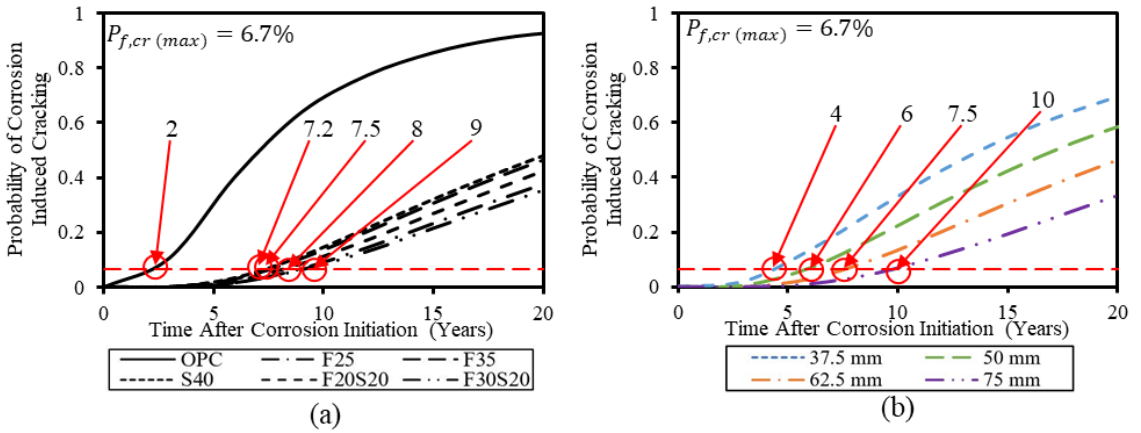

Fig. 7. Time-variant probabilities of failure ($P_{f(cr)}$) for the propagation period for (a) All mixes considered and cover of 62.5 mm and (b) All covers considered and F35 mix for *w/b* ratio=0.46.

Many service life estimations often ignore T_{cr}, and consider T_i as the end of the functional service life [18]. However, as discernible from the discussion above, T_{cr} can substantially add to the overall functional lifespan of RC structures by adopting greater cover depths and optimal binder types. Given the increasing emphasis on sustainable construction practices, encompassing reduced lifetime costs, CO_2 emissions, and improved maintenance and repair strategies, the time to corrosion induced cracking plays a pivotal role in extending the service life of RC structures and warrants inclusion in total service life estimations.

7.3 Illustrative Example

The results of the service life analysis presented before have laid the premises for the estimation of LCC and lifetime CO_2-e for coastal RC structures. The functional unit is a standard counterfort retaining wall (**Fig. 8**), with the LCC analysis conducted per meter length. Initial construction costs and embodied CO_2 are estimated from the wall's geometric dimensions, assuming concrete with a 28-day compressive strength equal to the design strengths considered in this study and reinforcement with a yield strength of at least 413 MPa (Grade 60). The geometric dimensions are detailed in **Fig. 8.**

Following the cracking of the concrete cover, 'patchwork' repair is carried out by replacing the damaged concrete above the reinforcement with fresh concrete. The repair concrete used for patchwork is assumed to possess a similar quality to the original concrete. The corrosion rate and, consequently, the crack propagation period have been assumed to be similar for patchworks. It's assumed that 10% of the area requires repair at each interval [11]. While patchwork is ongoing, reinforcement degradation continues uniformly. Once the reinforcement area reduces by more than 10% [11], patchwork stops, and the structure is considered to have reached its ultimate limit state (ULS). For the purpose of analysis, the diameter of the main reinforcement is considered as 10 mm. Note that the design service life of the structure is considered to be 50 years, as suggested by the fib guidelines [42] for common civil engineering structures. **Fig. 9** presents an illustration of the aforementioned principles in approximating the repair frequencies for each alternative in the 28 MPa design strength category (*w/b* ratio = 0.46). In **Fig. 9d**, the probability of de-passivation ($P_{f(i)}$) reaches 10% nearly 11 years after construction for the S40 mix. At that point in time, the reinforcement area begins to reduce at a uniform rate in accordance with the calculated uniform corrosion rate. The probability of failure for the propagation period ($P_{f(cr),max}$) occurs after 18 years of the construction of the structure, marking the appearance of the first crack. Routine patchwork continues at an interval of 7 years (equal to T_{cr}) until the 50-year service life is reached. Within this period, the reinforcement area has been reduced by nearly 5%, which means the structure does not reach its ULS within 50 years.

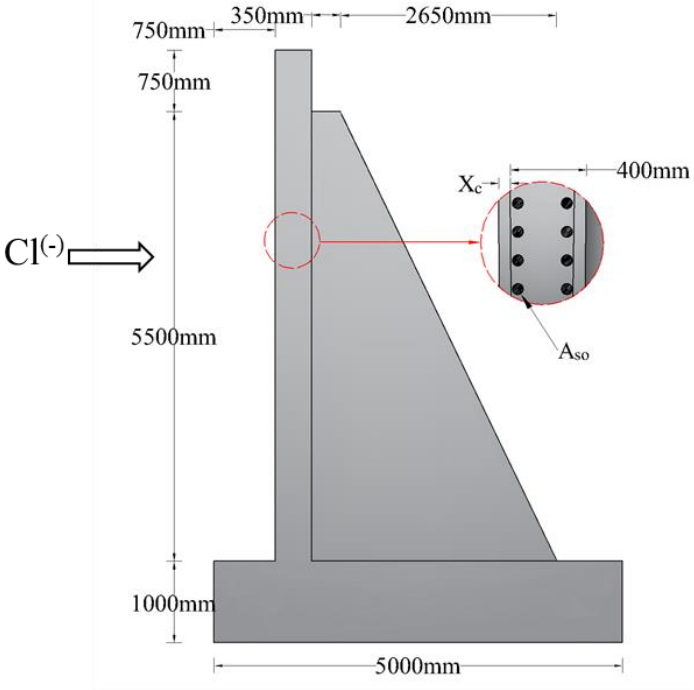

Fig. 8. Layout of the retaining wall considered.

From the criteria discussed above, it is possible to calculate the number of 'patchwork(s)' required for a structure till it reaches the ULS or the design service life of 50 years. When the patchwork is applied, it is assumed that the serviceability performance of the structure is restored, but the reinforcement degradation continues at a uniform rate. From **Fig. 9**, only OPC reaches the ULS among the considered mixes 31 years after construction, warranting the highest number of repairs of 15. Aligned with the service life analysis results, the F25 mix performs most satisfactorily, warranting no repairs in the 50-year period (**Fig. 9b**). Among the other mixes with SCMs, S40 requires the highest number of patchworks, i.e., 5 (**Fig. 9d**). **Fig. 10** shows the impact of concrete cover on reducing repair frequency. For the F35 mix, a 37.5 mm cover required 11 patchworks over 50 years, which dropped to 6 with a 50 mm cover. Increasing the cover to 62.5 mm reduced repairs to 1, and a 75 mm cover eliminated the need for patchwork altogether. **Fig. 9** and **Fig. 10** indicate that the reinforcement area reduces at a different rate for the different mixes, as well as for the various covers considered. Since the corrosion rate varies in accordance with the resistivity values of the different mixes, as well as the cover

thicknesses, the slope of the solid red line varies as well.

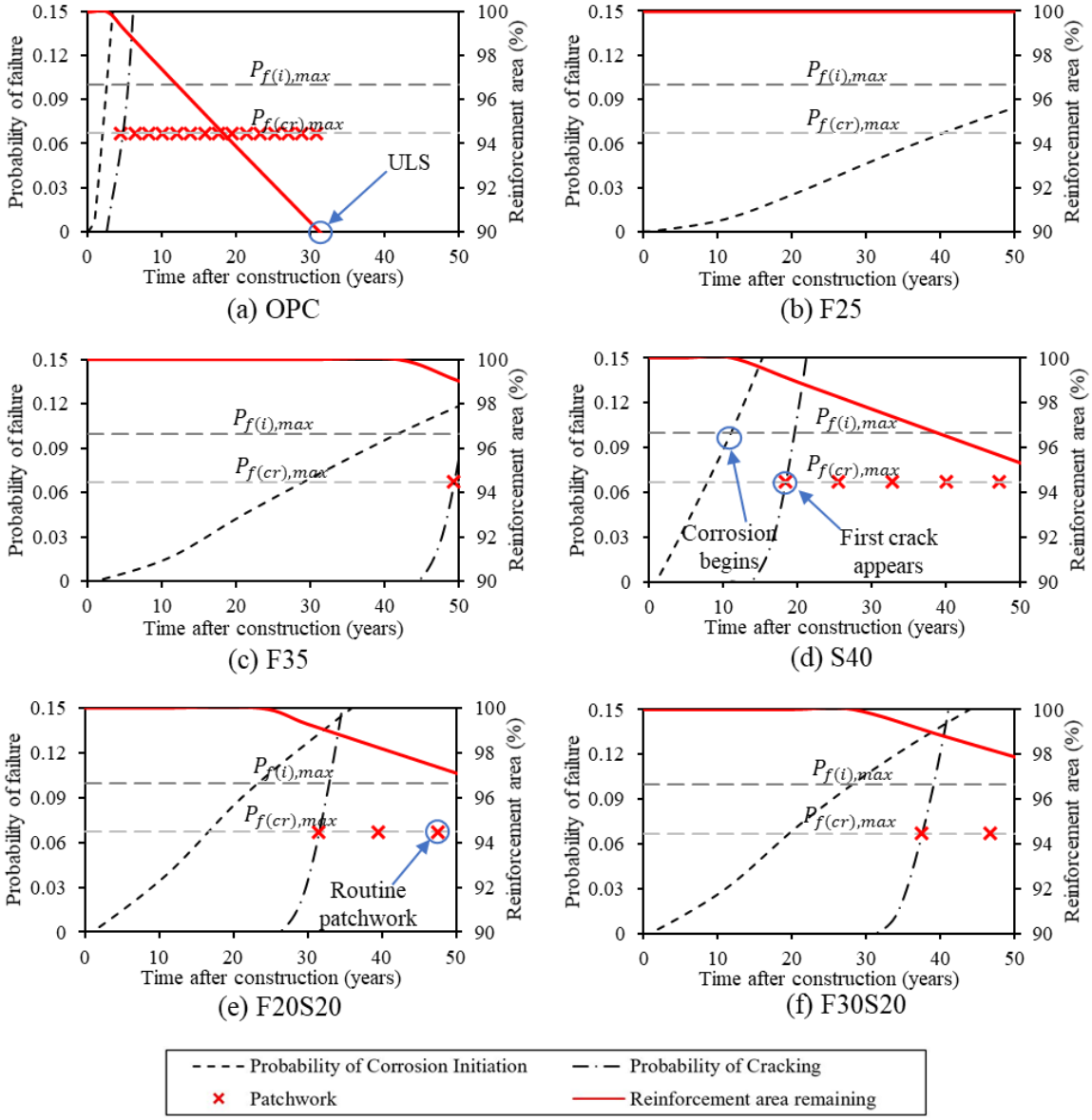

Fig. 9. Time-variant failure probabilities for the limit states of initiation and cracking and variation of percent area remaining of main reinforcement with time for a cover thickness of 62.5 mm, considering a service life of 50 years and *w/b* ratio = 0.46.

The analysis reveals that only OPC reaches the ULS for all the covers considered, across all three design strengths. For a 75 mm cover thickness, only S40 requires patchwork among all other SCM mixes, indicating that this cover may be unnecessary for a 50-year service life structure, given the binder types are chosen based on performance requirements. Furthermore, for the high *w/b* ratio = 0.57, only the F25 mix does not reach the ULS within the 50-year design service life for a 37.5 mm cover, necessitating the importance of cover thickness for local construction practices, particularly where construction quality control may be inconsistent.

7.4 Life Cycle Cost (LCC) Analysis

In order to conduct the LCC analysis, the retaining wall (**Fig. 8**) is considered to be constructed of the different mixes considered in this study, which are OPC, F25, F35, S40, F20S20, and F30S20, having specified design strengths of 35 MPa, 28 MPa, and 21 MPa. The main flexural reinforcement is considered to be of 10 mm diameter, the cross-sectional area of which is depicted by 'A_{so}' in **Fig. 8**.

For cost estimation in local rates, 'Schedule of Rates, 2022', published by the Public Works Department (PWD), Bangladesh, is used [76]. The standard "Schedule of Rates" indicates only a minor price difference between CEM I and CEM II binders. Given this, a conservative assumption was adopted wherein SCM mixes were considered to have equivalent cost to the OPC mixes. It should be noted that the cost analysis presented is indicative and intended to demonstrate potential LCC benefits of SCM mixes. In practice, where SCMs are available at lower costs, the sustainability advantage would likely be greater. The cost of concrete is \$178 per m^3 and the cost of reinforcement is \$1.11 per kg of steel [76]. The cost of each patchwork is approximately \$150 per m^2 including materials and subsidiary construction costs (labor, transportation, formwork, removal of existing concrete, surface preparation, etc.); which are assumed to be 1.5 times the material cost [12]. The cost of patchwork was estimated based on repair costs of concrete from the "Schedule of Rates", average depth of repair, and an overall multiplication factor of 2.5 applied to the material cost, considering the additional construction related costs.

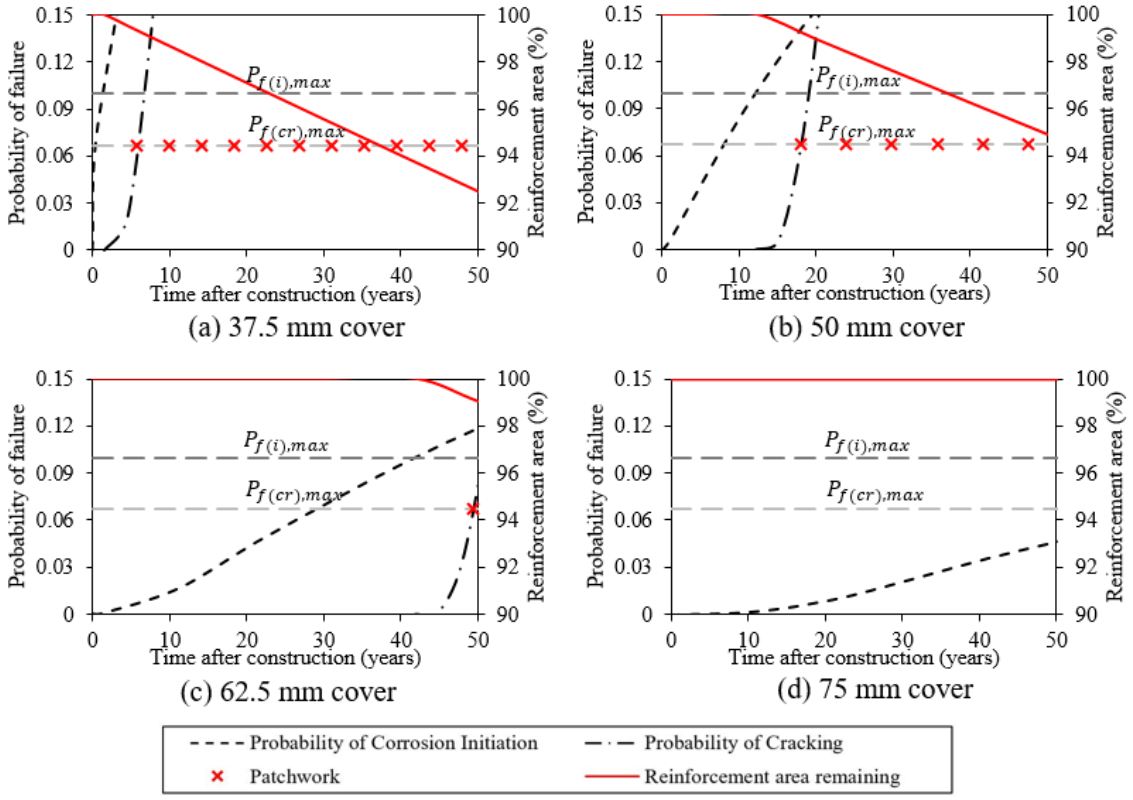

Fig. 10. Time-variant failure probabilities for the limit states of initiation and cracking and variation of percent area remaining of main reinforcement with time for F35 mix considering a service life of 50 years and *w/b* ratio = 0.46.

The time-variant LCC of the retaining wall (**Fig. 8**) for a 50-year period is calculated using Eq. (12), with the results shown in **Fig. 11** for the 28 MPa design strength. The LCCs for all alternatives have been expressed relative to the initial construction cost (C_c). **Fig. 11** indicates that OPC mixes, for all covers, reach the ULS within the design 50-year service life and have significantly higher LCCs compared to other mixes, demonstrating that SCM incorporated binders are more economical. OPC has higher LCCs compared to the SCM mixes, and the latter can sustain the incurred costs to under $1.5C_c$ to $2C_c$ for higher covers of 62.5 mm (**Fig. 11c**). The LCCs for F25, F35, F20S20, and F30S20 mixes exhibit flat line for 75 mm cover (**Fig. 11d**), which is true for the 21 MPa and 35 MPa mixes as well. It is to be noted that the fly ash mixes exhibit superior performance in terms of LCC than OPC and slag mixes due to the pozzolanic action of the active silica present. However, since the SCM mixes in general outperform OPC by substantial margins, the designer has the choice to select the appropriate SCM for replacement based on local availability, prices, and early strength requirements, given the clear cover is chosen accordingly as well.

Increasing cover thickness significantly reduces LCCs for the same concrete mix, as shown in **Fig. 12** (LCC per year with varying cover thickness, for the 28 MPa mixes). It is to be noted that this analysis is appropriate for a 50-year service life and would be different in the case of a 100-year or 75-year service period. Since the service life of OPC mixes terminated before the 50-year design period, the LCCs have been expressed as the average yearly LCC in **Fig. 12**, calculated by dividing cumulative costs by years in service and normalized to C_c. This provides an insight into the economic implications of various cover thicknesses, elucidating the impact of variable covers on the structure's overall cost effectiveness and maintenance costs throughout its lifespan in extreme saline exposure. **Fig. 12** shows that for the 28 MPa strength class, the average LCC/year decreases significantly for OPC mix and for SCM mixes, reducing to only 2% of C_c with increasing cover. Incorporating appropriate SCMs with a cover of 62.5 mm or 75 mm can reduce the yearly LCC significantly.

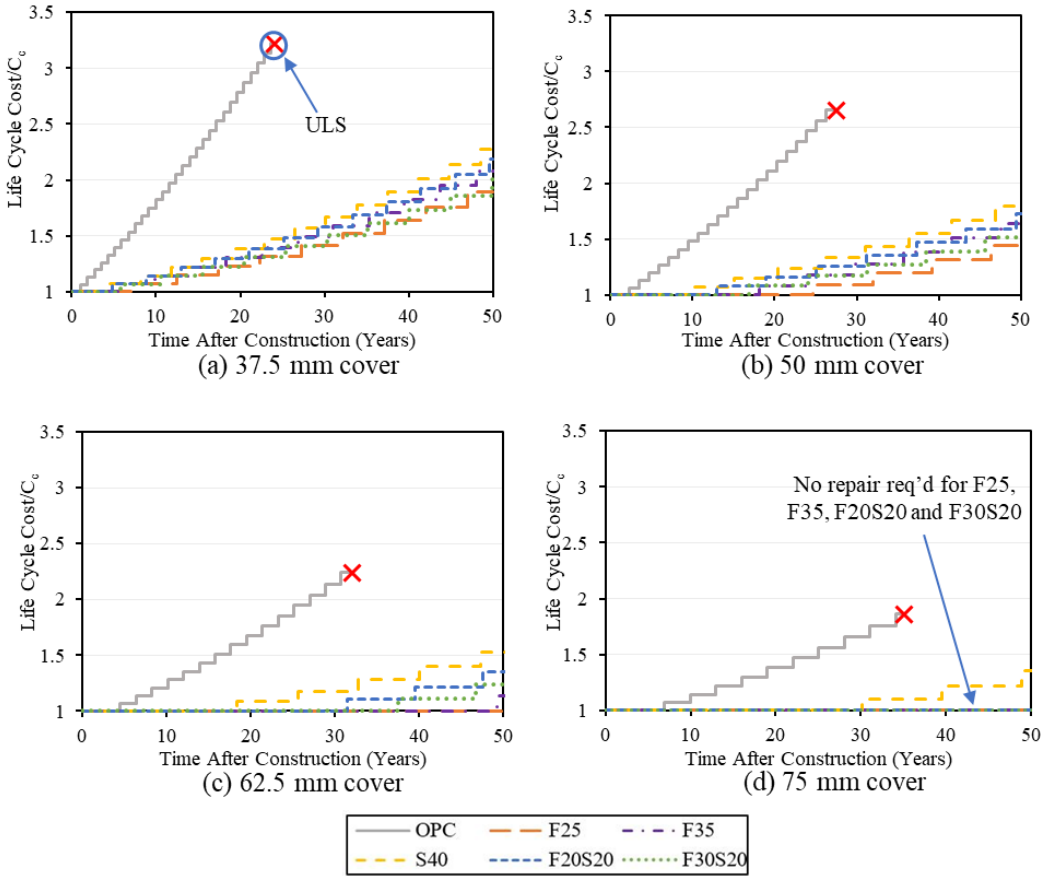

Fig. 11. Time-variant LCC per meter of the retaining wall with respect to the initial construction cost (C_c) for *w/b* ratio = 0.46.

7.5 Equivalent Emissions (in CO_2-e)

Based on Eq. (13) and **Fig. 13**, the lifetime CO_2 emissions (kg CO_2-e) for the 28 MPa design strength mixes show that while emissions decrease with increasing cover, in line with the results from the LCC analysis and the estimated repair frequencies, the carbon footprint of the retaining wall considered mostly varies with respect to the cement replacement. For a 37.5 mm cover, the mix without cement replacement has the highest emissions at 7215 kg CO_2-e, which reduces by over half to about 3230 kg CO_2-e for the F30S20 mix.

Increasing concrete cover from 37.5 mm to 75 mm reduces the frequency of repairs and the carbon footprint, particularly for mixes with higher cement replacement. As a result, the combination of cover increment and cement replacement produces far less kg CO_2-e than the OPC mixes for all strength classes. For instance, in the 28 MPa mixes, the lifetime CO_2-e emissions reduce from 7215 kg CO_2-e (OPC, 37.5 mm) to only 2325 kg CO_2-e (F30S20, 75 mm); and this pattern is true for the other design

strengths as well. However, the embodied emissions increase slightly with increasing cover from 62.5 mm to 75 mm for the F25 mix, which is due to the fact that the structure warrants no repair in its service life at 62.5 mm. Despite incorporating a larger cover thickness results in a higher volume of concrete consumption and consequently, a higher carbon footprint, the higher cover is clearly beneficial in reducing repair operations and lifetime CO_2-e emissions of RC structures under chloride exposure.

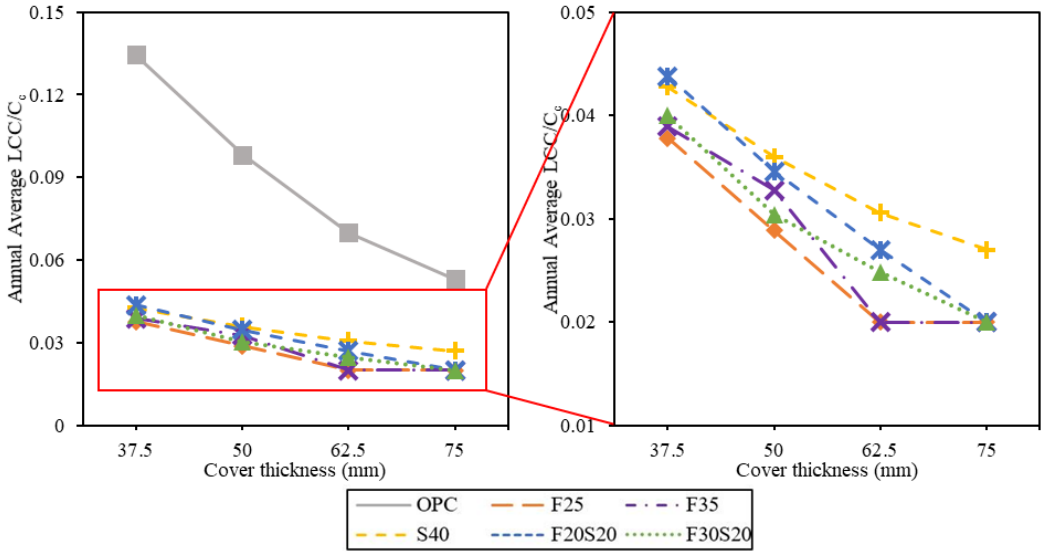

Fig. 12. LCC per year of service life with increasing cover thickness with respect to initial construction cost (C_c) for *w/b* ratio = 0.46.

Fig. 14 illustrates that lifetime CO_2 emissions generally increase as the water-binder (*w/b*) ratio decreases, meaning higher design strengths lead to greater emissions [77]. This is primarily due to the higher cement content required for stronger concrete, as cement is the main source of embodied emissions. Additionally, all of the SCM mixes show significantly low CO_2-e compared to their OPC counterparts. This presents a trade-off between higher design strengths (lower *w/b* ratio) and lower carbon emissions, both for mixes with and without SCMs. However, the trade-off can be mitigated by selecting an optimum mix; for example, the F30S20 mix displays a lower carbon footprint compared to the F25 mix at all *w/b* ratios. The total reduction in embodied CO_2-e is around 60% for the F30S20 mix, with the reduction ranging up to 70% for low-strength-high-cover alternatives. Thus, the engineer can make the choice of selecting a higher design strength for his/her structure, at the expense of higher embodied emissions. Conversely, selecting a high-strength mix will eventually lead to reduced section sizes, which will ultimately lower the volume of concrete produced, lowering the lifetime CO_2-e.

7.6 Material Sustainability Indicators (MSI)

Material Sustainability Indicators (MSI) have been defined as the compressive strength per unit of LCC per C_c and the compressive strength per unit of embodied CO_2-e. While the proposed MSIs are not yet standardized compared to global sustainability indices, they are consistent with broader sustainability assessment principles used in performance-based design. Similar metrics have also been employed in previous research [78]. In this study, MSIs serve as comparative tools to support mix optimization and integrate both efficiency and environmental considerations. The MSIs have been illustrated in **Fig. 15** with varying *w/b* ratios for two design covers (37.5 mm and 62.5 mm). Since the specified design strengths of 35 MPa, 28 MPa, and 21 MPa have been achieved for all binder alternatives at later ages, these values are used to calculate the MSIs. As cover increases, both strength per unit LCC and CO_2-e increase across all binder types due to reduced repair frequency. The F25 and F35 mixes have the highest strength per unit LCC, while the OPC mix has the lowest, driven by its higher permeability and repair needs. Considering the embodied CO_2-e per unit compressive strength, the F30S20 mix performs the best, due to the combined effect of the high volume replacement and the reduced number of repair intervals owing to the pozzolanic activity of fly ash and slag. At lower design strengths and higher cover, fly ash-only mixes are sustainable options as well compared to OPC mixes.

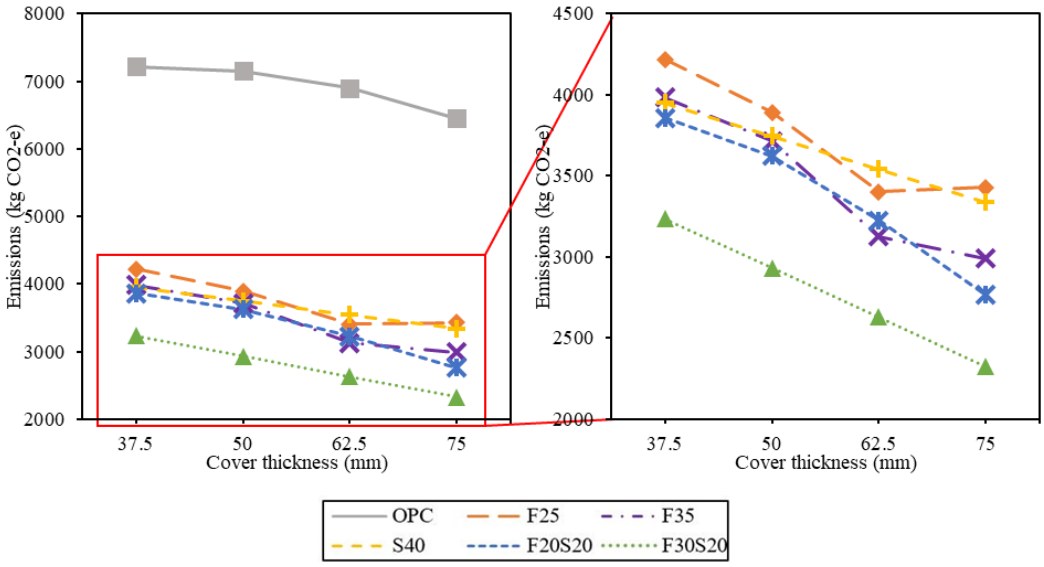

Fig. 13. Total CO_2 emissions with increasing cover thickness per meter of the retaining wall considering 50-year design service life for *w/b* ratio = 0.46.

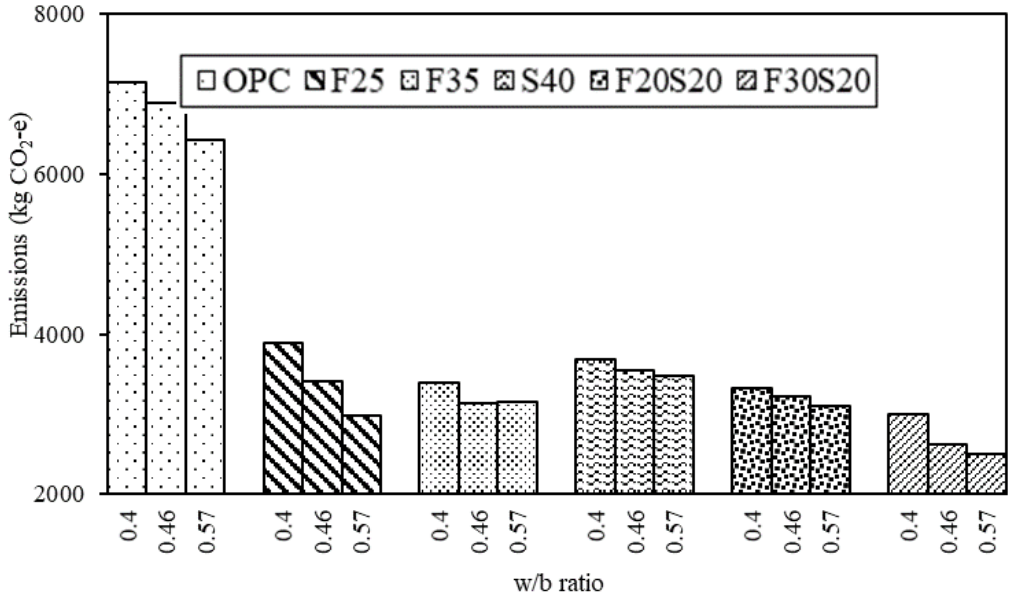

Fig. 14. Total CO_2 emissions with varying water-binder ratios per meter of the retaining wall, considering 50-year design service for 62.5 mm cover.

Fig. 15 reports that as design strength decreases, the MSIs decrease. This occurs mainly due to defining the MSIs as compressive strength per unit of LCC per C_c or embodied CO_2. For example, the MSIs for the 21 MPa mixes (*w/b* = 0.57) are much lower than for 35 MPa mixes (*w/b* = 0.40). A higher MSI value signifies more efficient concrete usage. Higher strength allows for reduced section sizes, reducing the overall volume, cost, and CO_2 emissions. Moreover, the higher strength mixes offer superior durability with a longer service life and fewer repairs. Despite the higher cement content and corresponding carbon emissions, the high-strength concrete is the better choice for minimizing lifecycle costs and lifetime embodied emissions. Regarding the trade-off between higher strength and lower carbon emissions, the MSI values could be used as pointers for an optimum mix. For example, for a 37.5 mm cover, the F30S20 mix exhibits high values for both MSIs, with the MSI (Embodied CO_2) increasing with lower *w/b* ratios, in contrast to the results in **Fig. 14**. This illustrates the importance of SCM optimization and higher-strength concrete for producing sustainable and economic structures.

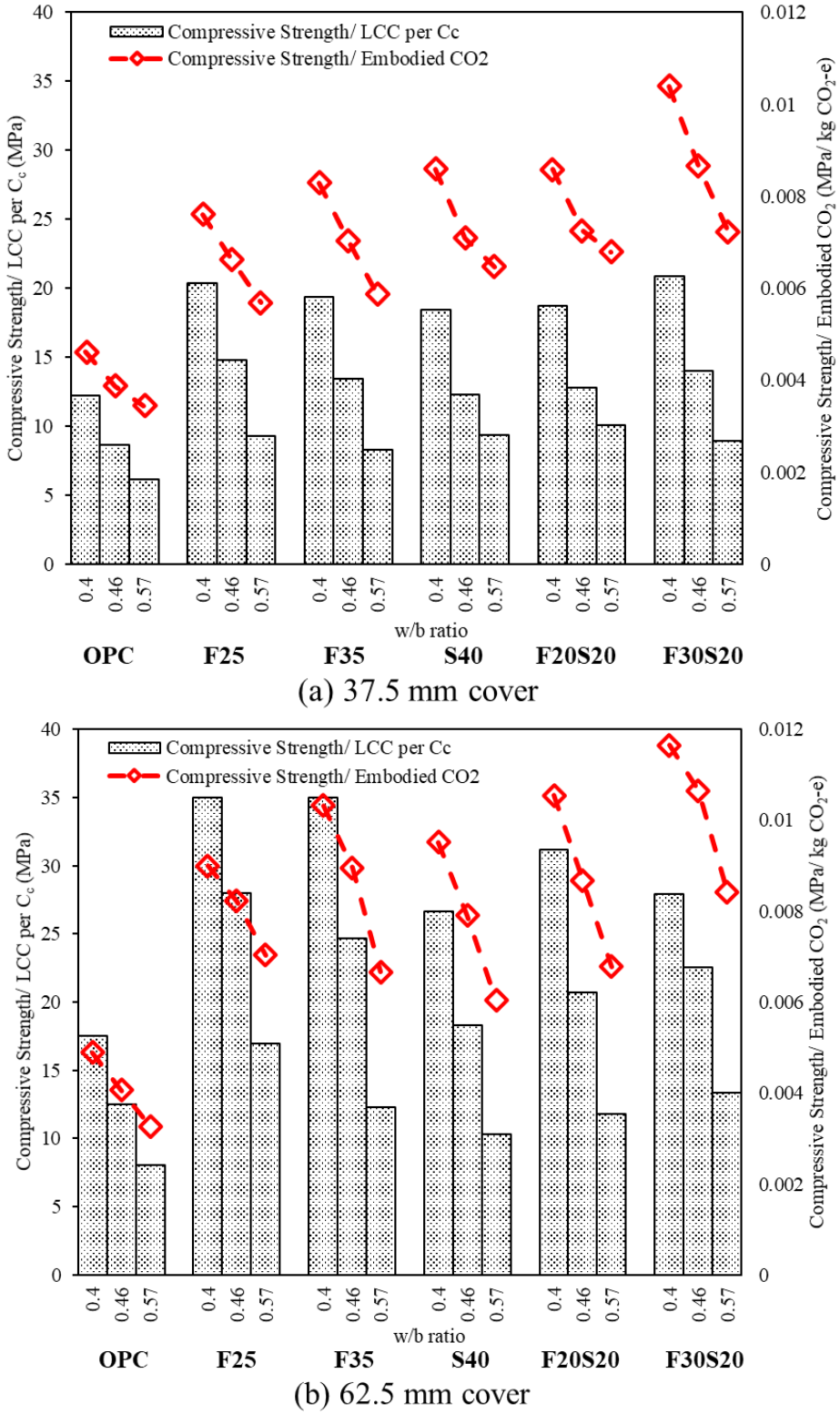

Fig. 15. Material Sustainability Indicators (MSI) with varying *w/b* ratios and (a) 37.5 mm cover and (b) 62.5 mm cover.

8 Conclusions

This study introduces a probabilistic performance-based framework to predict and compare the service life, life-cycle cost (LCC), and embodied carbon emissions (in kg CO_2-e) of various concrete mixes in harsh marine exposures. In this study, a framework is presented for the sustainability performance comparison of different common binder types used for the construction and repair of RC

structures, combined with the impact of clear covers. The analysis has been conducted on a typical counterfort retaining wall as a case study. For each design alternative, the time-variant failure probabilities have been computed. Finally, the LCC for each alternative has been computed and compared. Based on the analysis results and discussion, the following conclusions can be drawn.

- Incorporating SCMs significantly extends the service life (T_L) of mixes, with slag mixes outperforming OPC mixes and F25 mixes providing the greatest durability across all design strengths. The T_L of various alternatives has also been found to be highly sensitive to increasing clear covers. For example, for the 28 MPa design strength, T_L increased from 7.5 years to around 70 years as cover thickness increased from 37.5 mm to 62.5 mm, a nearly ten-fold increase.
- In the case study examined, only OPC reached its Ultimate Limit State (ULS) within 50-years of service period for all covers and design strengths considered, requiring the highest number of repairs despite its shorter service life compared to SCM mixes. Increasing concrete cover significantly reduced the need for repairs across all mixes.
- Incorporating SCMs and ensuring adequate concrete cover effectively lowers the LCC in OPC mixes. Fly ash replacement proves most effective compared to slag alone.
- Although lifetime CO_2-e emissions reduce with increasing cover for all the binder types, the carbon footprint of the structure primarily reduces with increasing cement replacement. Hence, the F30S20 mixes perform the best in this regard. However, for each particular mix, the total embodied emission increases with respect to increasing design strength.
- The Material Sustainability Indicators (MSI) illustrate that by optimally combining binder types and cover thickness, the F25 mix results in the highest Compressive Strength/ LCC per C_c for all design strengths. The Compressive Strength/ Embodied Emissions generally show optimal values for the F30S20 mix, due to its high volume binder replacement. At lower design strengths and higher cover, fly ash-only mixes are sustainable options as well. The higher strength mixes are more efficient in minimizing LCC and lifetime CO_2 emissions.

The findings from this study are limited to the particular case study and a design service life of 50 years. However, the analysis conducted shows a quantitative comparison of the service life values, LCCs, and environmental impact of concrete mixes with a wide range of binder types and varying covers, providing a basis for stakeholders to implement policy decisions based on performance-based design guidelines.

Acknowledgement

The authors are also thankful to the staff of the Concrete Laboratory of Department of Civil Engineering, BUET for their cooperation.

Funding Statement

The authors would like to acknowledge the financial support provided by the Research and Innovation Centre for Science and Engineering (RISE), BUET (Project ID: 2022-02-060) for this research work.

CRediT authorship contribution statement

Sakib Hasnat: Investigation, Formal analysis, Writing – original draft. **Tanvir Manzur**: Conceptualization, Supervision, Writing – review & editing.

Conflicts of Interest

The authors declare that they have no conflicts of interest to report regarding the present study.

Data Availability Statement

Some or all data, models, or codes that support the findings of this study are available from the corresponding author upon reasonable request.

References

[1] Zhou Y, Gencturk B, Willam K, Attar A. Carbonation-Induced and Chloride-Induced Corrosion in Reinforced Concrete Structures. Journal of Materials in Civil Engineering 2015; 27(9): 04014245. https://doi.org/10.1061/(ASCE)MT.1943-5533.0001209.

[2] Manzur T, Baten B, Hasan MJ, Akter H, Tahsin A, Hossain KMA. Corrosion behavior of concrete mixes with masonry chips as coarse aggregate. Construction and Building Materials 2018; 185: 20–29. https://doi.org/10.1016/j. conbuildmat.2018.07.033.

[3] Koch G. Cost of corrosion. Trends in Oil and Gas Corrosion Research and Technologies 2017; 3–30. https://doi.org/10.1016/B978-0-08-101105-8.00001-2.

[4] Medeiros-Junior RA, Reichert TA. Impact of climate change on the service life of concrete structures. Eco-Efficient Repair and Rehabilitation of Concrete Infrastructures 2018; 43–68. https://doi.org/10.1016/B978-0-08-102181-1.00003-4

[5] Rumman R, Kamal MR, Manzur T, Noor MA. Durability Performance of Locally Produced OPC and PCC Cement Concretes. International Conference on Recent Innovation in Civil Engineering for Sustainable Development (IICSD-2015) 2015; Dep. Civ. Eng. DUET - Gazipur, Bangladesh. 1–6. https://doi.org/10.13140/RG.2.1.2463.1128.

[6] Tuutti K. Service Life of Structures with Regard to Corrosion of Embedded Steel. ACI Symposium Publication 1980; 65: 223-226. https://doi.org/10.14359/6355.

[7] Angst UM, Elsener B, Larsen CK, Vennesland Ø. Critical chloride content in reinforced concrete - A review. Cement and Concrete Research 2009; 39(12): 1122–1138. https://doi.org/10.1016/j.cemconres. 2009.08.006.

[8] Angst UM. Challenges and opportunities in corrosion of steel in concrete. Materials and Structures 2018; 51(4). https://doi.org/10.1617/s11527-017-1131-6.

[9] Huntzinger DN, Eatmo TD. A life-cycle assessment of cement manufacturing: comparing traditional process with alternative technologies. Journal of Cleaner Production 2009; 17(7): 668–75. https://doi.org/10.1016/j.jclepro.2008.04.007

[10] Yang KH, Jung YB, Cho MS, Tae SH. Effect of supplementary cementitious materials on reduction of CO2 emissions from concrete. Journal of Cleaner Production 2015; 103: 774–783. https://doi.org/10.1016/j.jclepro.2014.03.018.

[11] Sajedi S, Huang Q. Reliability-based life-cycle-cost comparison of different corrosion management strategies. Engineering Structures 2019; 186(1): 52–63. https://doi.org/10.1016/j.engstruct.2019.02.018.

[12] Liu G, Hua J, Wang N, Deng W, Xue X. Material Alternatives for Concrete Structures on Remote Islands: Based on Life-Cycle-Cost Analysis. Advances in Civil Engineering 2022; 2022: 7329408. https://doi.org/10.1155/2022/7329408.

[13] O'Reilly M, Darwin D, Browning J, Locke Jr CE. Evaluation of multiple corrosion protection systems for reinforced concrete bridge decks. University of Kansas Center for Research, Inc., 2011.

[14] Younis A, Ebead U, Judd S. Life cycle cost analysis of structural concrete using seawater, recycled concrete aggregate, and GFRP reinforcement. Construction and Building Materials 2018; 175: 152–160. https://doi.org/10.1016/j.conbuildmat.2018.04.183.

[15] Wittocx L, Buyle M, Audenaert A, Seuntjens O, Renne N, Craeye B. Revamping corrosion damaged reinforced concrete balconies: Life cycle assessment and life cycle cost of life-extending repair methods. Journal of Building Engineering 2022; 52(3): 104436. https://doi.org/10.1016/j.jobe.2022.104436.

[16] Papakonstantinou KG, Shinozuka M. Probabilistic model for steel corrosion in reinforced concrete structures of large dimensions considering crack effects. Engineering Structures 2013; 57: 306–326. https://doi.org/10.1016/j. engstruct.2013.06.038.

[17] Nogueira CG, Yoshio L, Zacchei E. Deterministic and probabilistic approaches for corrosion in RC structures: A direct proposed model to total service life predictions. Case Studies in Construction Materials 2023; 18(2): e01913. https://doi.org/10.1016/j.cscm.2023.e01913.

[18] Petcherdchoo A. Repairs by fly ash concrete to extend service life of chloride-exposed concrete structures considering environmental impacts. Construction and Building Materials 2015; 98: 799–809. https://doi.org/10.1016/j.conbuildmat.2015.08.120.

[19] Petcherdchoo A. Probability-Based Sensitivity of Service Life of Chloride-Attacked Concrete Structures with Multiple Cover Concrete Repairs. Advances in Civil Engineering 2018; 2018: 1–17. https://doi.org/10.1155/2018/4525646.

[20] Menna Barreto MFF, Timm JFG, Passuello A, Dal Molin DCC, Masuero JR. Life cycle costs and impacts of massive slabs with varying concrete cover. Cleaner Engineering and Technology 2021; 5: 100256.

https://doi.org/10.1016/j.clet.2021.100256.
[21] Val DV, Stewart MG. Life-cycle cost analysis of reinforced concrete structures in marine environments. Structural Safety 2003; 25(4): 343–362. https://doi.org/10.1016/S0167-4730(03)00014-6.
[22] Hasnat S, Rafiuzzaman S, Baten B, Manzur T. Carbonation Susceptibility of Reinforced Concrete Structures: A review. Proceedings of 5th Annual Paper Meet and Civil Engineering Congress, Dhaka, Bangladesh 2022: 218-263.
[23] Baten B, Manzur T, Ahmed I. Combined effect of binder type and target mix-design parameters in delaying corrosion initiation time of concrete. Construction and Building Materials 2020; 242: 118003. https://doi.org/10.1016/j.conbuildmat.2020.118003
[24] Torsha T, Manzur T, Chowdhury NR, Hasan MJ. Significance of integrating probabilistic performance-based cover design in local construction guidelines for adequate serviceability of coastal built environment: Bangladesh perspective. Natural Hazards 2022; 112(1): 919–946. https://doi.org/10.1007/s11069-022-05213-1.
[25] ACI. ACI PRC-232.2-18: Report on the Use of Fly Ash in Concrete. American Concrete Institute 2018; Farmington Hills, MI, USA.
[26] ACI 211. Standard Practice for Selecting Proportions for Normal Heavyweight and Mass Concrete 1991; American Concrete Institute, Michigan.
[27] ASTM C127. Standard test method for Density, Relative Density (Specific Gravity) and Absorption of Coarse Aggregate. American Society for Testing and Materials 2007.
[28] ASTM C128. Standard test method for Density, Relative Density (Specific Gravity) and Absorption of Coarse Aggregate. American Society for Testing and Materials 2009.
[29] ASTM C29. Standard Test Method for Bulk Density (‘‘Unit Weight’) and Voids in Aggregate. American Society for Testing and Materials 2009.
[30] BS 812. Testing Aggregates: Methods for determination of particle size and shape, British Standards Institutions 1975; 2 Park Street, London W1A 2BS.
[31] ASTM C131. Standard Test Method for Resistance to Degradation of Small-Size Coarse Aggregate by Abrasion and Impact in the Los Angeles Machine. American Society for Testing and Materials 2003.
[32] ASTM C136. Standard Test Method for Sieve Analysis of Fine and Coarse Aggregates. American Society for Testing and Materials 2006.
[33] ASTM C143. Standard Test Method for Slump of Hydraulic-Cement Concrete. American Society for Testing and Materials 2015.
[34] ASTM C39 – 14a. Standard Test Method for Compressive Strength of Cylindrical Concrete Specimens. American Society for Testing and Materials 2014.
[35] NT Build 492. Concrete, mortar and cement-based repair materials: Chloride migration coefficient from non-steady-state migration experiments. NORDTEST 1999; Finland.
[36] Spragg RP, Bu Y, Snyder KA, Bentz DP, Weiss J. Electrical Testing of Cement-Based Materials: Role of Testing Techniques, Sample Conditioning, and Accelerated Curing 2013. https://doi.org/10.5703/1288284315230.
[37] Wenner F. A method of measuring earth resistivity. Bulletin of the National Bureau of Standards 1916; 469–478.
[38] AASHTO T 358-15. Standard Method of Test for Surface Resistivity Indication of Concrete’s Ability to Resist Chloride Ion Penetration. American Association of State Highway and Transportation Officials 2015; Washington, DC.
[39] Spragg RP, Villani C, Snyder KA, Bentz DP, Bullard J, Weiss J. Factors that influence electrical resistivity measurements in cementitious systems. Transportation Research Record 2013; 11(2342): 90–98. https://doi.org/10.3141/2342-11.
[40] Weiss J, Snyder KA, Bullard J, Bentz DP. Using a Saturation Function to Interpret the Electrical Properties of Partially Saturated Concrete. Journal of Materials in Civil Engineering 2013; 25(8): 1097–1106. https://doi.org/10.1061/(asce)mt.1943-5533.0000549.
[41] Baten B, Manzur T. Formation Factor Concept for Non-Destructive Evaluation of Concrete’s chloride diffusion coefficients. Cement and Concrete Composites 2022; 128(12):104440. https://doi.org/10.1016/j.emconcomp.2022.104440.
[42] Fib. Bulletin 34: Model code for service life design. Fib 2006; Lausanne.
[43] Fib. Bulletin 76: Benchmarking of deemed to satisfy provisions in standards: durability of reinforced concrete structures exposed to chlorides. Fib 2015; Lausanne.
[44] Rengaraju S, Pillai RG, Gettu R. Input parameters and nomograms for service life-based design of reinforced concrete structures exposed to chlorides. Structures 2023; 56(7): 104847. https://doi.org/10.1016/j.istruc.2023.07.037.
[45] NASA Power Data Access Viewer. https://power.larc.nasa.gov/data-access-viewer/, 2023 (accessed on 23 October 2023).

[46] El Maaddawy T, Soudki K. A model for prediction of time from corrosion initiation to corrosion cracking. Cement and Concrete Composites 2007; 29(3): 168–175. https://doi.org/10.1016/j.cemconcomp.2006.11.004.
[47] Chernin L, Val DV, Volokh KY. Analytical modelling of concrete cover cracking caused by corrosion of reinforcement. Materials and Structures 2010; 43(4): 543–556. https://doi.org/10.1617/s11527-009-9510-2
[48] Bhargava K, Ghosh AK, Mori Y, Ramanujam S. Model for cover cracking due to rebar corrosion in RC structures. Engineering Structures 2006; 28(8): 1093–1109. https://doi.org/10.1016/j.engstr uct.2005.11.014.
[49] Balafas I, Burgoyne CJ. Modeling the Structural Effects of Rust in Concrete Cover. Journal of Engineering Mechanics 2011; 137(3): 175–185. https://doi.org/10.1061/(asce)em.1943-7889.0000215.
[50] Liang Y, Wang L. Prediction of corrosion-induced cracking of concrete cover: A critical review for thick-walled cylinder models. Ocean Engineering 2020; 213(7): 107688. https://doi.org/10.1016/j.oceaneng.2020.107688.
[51] Chen F, Baji H, Li CQ. A comparative study on factors affecting time to cover cracking as a service life indicator. Construction and Building Materials 2018; 163: 681–694. https://doi.org/10.1016/j.conbuildmat.2017.12.120.
[52] Timoshenko S. Strength of Materials. Part II: Advanced Theory and Problems, 3rd ed 1956; Princeton, New Jersey, New York: D. Van Nostrand Company, Inc.
[53] Pour-Ghaz M, Isgor OB, Ghods P. The effect of temperature on the corrosion of steel in concrete. Part 1: Simulated polarization resistance tests and model development. Corrosion Science 2009; 51(2): 415–425. https://doi.org/10.1016/j.corsci.2008.10.034.
[54] Hornbostel K, Larsen CK, Geiker MR. Relationship between concrete resistivity and corrosion rate - A literature review. Cement and Concrete Composites 2013; 39: 60–72. https://doi.org/10.1016/j.cemconcomp.2013.03.019.
[55] Pour-Ghaz M, Isgor OB, P. Ghods P. The effect of temperature on the corrosion of steel in concrete. Part 2: Model verification and parametric study. Corrosion Science 2009; 51: 426–433. https://doi.org/10.10106/j.corsci.2008.10.036
[56] Valipour M, Shekarchi M, Ghods P. Comparative studies of experimental and numerical techniques in measurement of corrosion rate and time-to-corrosion-initiation of rebar in concrete in marine environments. Cement and Concrete Composites 2014; 48: 98–107. https://doi.org/10.1016/j.cemconcomp. 2013.11.001.
[57] DuraCreteR17. Final technical report, DuraCrete – probabilistic performance-based durability design of concrete structures. The European Union–Brite EuRam III, 2000 (Document BE95-1347/R17).
[58] ACI. Building Code Requirements for Structural Concrete (ACI 318-05) and Commentary (ACI 318R-05). American Concrete Institute 2005; Michigan.
[59] Xu Q, Shi D, Shao W. Service life prediction of RC square piles based on time-varying probability analysis. Construction and Building Materials 2019; 227: 116824. https://doi.org/10.1016/j.conbuildmat.2019.116824.
[60] ASTM E917. Standard Practice for Measuring Life-Cycle Costs of Buildings and Building Systems. American Society for Testing and Materials, 2017.
[61] Data Bank. The World Bank, https://databank.worldbank.org, 2023 (accessed on 2 December 2023).
[62] Sanal I. Discussion on the effectiveness of cement replacement for carbon dioxide (CO2) emission reduction in concrete. Greenhouse Gases: Science and Technology 2017; 8: 366-378. https://doi.org/10.1002/ghg.1748
[63] Turner LK, Collins FG. Carbon dioxide equivalent (CO2-e) emissions: A comparison between geopolymer and OPC cement concrete. Construction and Building Materials 2013; 43: 125-130. https://doi.org/10.1016/j.conbuildmat.2013.01.023.
[64] Petcherdchoo A. Environmental impacts of combined repairs on marine concrete structures. Journal of Advances in Concrete Technology 2015; 13: 205-213. https://doi.org/10.3151/jact.13.20
[65] Zhu X, Zhang Y, Liu Z, Qiao H, Ye F, Lei Z. Research on carbon emission reduction of manufactured sand concrete based on compressive strength. Construction and Building Materials 2023; 403: 133101. https://doi.org/10.1016/j.conbuildmat.2023.133101.
[66] Hasnat S, Rafiuzzaman S, Baten B, Manzur T. Half-Cell Potential Measurement as a Non-destructive Evaluation of Chloride Diffusion Coefficient. Lecture Notes in Civil Engineering 2024; 219–231. https://doi.org/10.1007/978-3-031-61511-5_18.
[67] Elahi A, Basheer PAM, Nanukuttan SV, Khan QUZ. Mechanical and durability properties of high performance concretes containing supplementary cementitious materials. Construction and Building Materials 2010; 24(3): 292–299. https://doi.org/10.1016/j.conbuildmat.2009.08.045.
[68] Hooton RD. Canadian use of ground granulated blast-furnace slag as a supplementary cementing material for enhanced performance of concrete. Canadian Journal of Civil Engineering 2000; 27(4): 754–760. https://doi.org/10.1139/l00-014.
[69] Rafiuzzaman S, Hasnat S, Baten B, Manzur T. Effect of binder types on corrosion potential of local concrete mixes of Bangladesh. Proceedings of the 5th annual paper meet and 2nd civil engineering congress 2022; 7: 29-30 Dhaka, Bangladesh.

[70] Chindasiriphan P, Yokota H, Pimpakan P. Effect of fly ash and superabsorbent polymer on concrete self-healing ability. Construction and Building Materials 2020; 233: 116975. https://doi.org/10.1016/j.conbuildmat.2019.116975.
[71] BNBC-Part 6, Chapter 8, Section 8.1. Bangladesh National Building Code, Detailing of Reinforced Concrete Structures. Housing and Building Research Institute, Bangladesh, 2006.
[72] Hasnat S, Rafiuzzaman S, Choudhury A, Baten B, Manzur T. Formation Factor as a Non-Destructive Measure of Chloride Diffusion Coefficient. In Proceedings of the 16th International Congress on the Chemistry of Cement (ICCC2023) 2023; 3: 309-402.
[73] Samrose S, Anzum S, Mahmud S, Manzur T. Tentative Optimum Proportion of Supplementary Cementitious Materials in Blended Cement to Perform Better under Tannery Wastewater. Materials Science Forum 2018; 937: 107–113. https://doi.org/10.4028/www.scientific.net/MSF.937.107.
[74] Marques PF, Costa A, Lanata F. Service life of RC structures: Chloride induced corrosion: Prescriptive versus performance-based methodologies. Materials and Structures 2012; 45(1–2): 277–296. https://doi.org/10.1617/s11527-011-9765-2.
[75] Hasnat S, Manzur T. Importance of Optimally Combining Binder Types and Rebar Cover in Reducing Lifetime CO2 Emissions in RC Structures. in The 1st International Conference on Net-Zero Built Environment, M. Kioumarsi and B. Shafei, Eds., Cham: Springer Nature Switzerland 2025; 673–685. https://doi.org/10.1007/978-3-031-69626-8_56.
[76] PWD. Schedule of Rates 2022; 2022(2). Public Works Department (PWD), Bangladesh, 2023.
[77] Scrivener KL, John VM, Gartner EM. Eco-efficient cements: Potential economically viable solutions for a low-CO2 cement-based materials industry. Cement and Concrete Research 2018; 114(12) 2–26. https://doi.org/10.1016/j.cemconres.2018.03.015.
[78] Yu J, Wu HL, Leung CKY. Feasibility of using ultrahigh-volume limestone-calcined clay blend to develop sustainable medium-strength Engineered Cementitious Composites (ECC). Journal of Cleaner Production 2020; 262(7) 121343. https://doi.org/10.1016/j.jclepro.2020.121343.